Macromolecules
ARTICLE

Macromolecules **2009**, *42*, 7203–7212 **7203**
DOI: 10.1021/ma901259j

Influence of Weak Attractive Interactions on Structures and Properties of Poly(trimethylene terephthalate)

Yuji Sasanuma* and Nobuaki Suzuki

Department of Applied Chemistry and Biotechnology, Faculty of Engineering, Chiba University, 1-33 Yayoi-cho, Inage-ku, Chiba 263-8522, Japan

Received June 12, 2009; Revised Manuscript Received July 20, 2009

ABSTRACT: Conformational analysis of poly(trimethylene terephthalate) (PTT) has been carried out by the refined rotational isomeric state (RIS) scheme with ab initio molecular orbital (MO) calculations for a model compound, trimethylene glycol dibenzoate (TMGDB). Bond conformations of the O−CH_2−CH_2−CH_2−O part of TMGDB were determined from ^{1}H and ^{13}C NMR experiments for unlabeled and ^{13}C-labeled TMGDBs. The MO calculations exactly reproduced not only the experimental bond conformations but also the dipole moment and molar Kerr constant observed from TMGDB dissolved in nonpolar solvents. Comparison of the MO calculations with and without electron correlations revealed that a variety of intramolecular attractions, such as $\pi-\pi$ interactions, electrostatic attractions, dipole−dipole interactions, and C═O···H−C and C−O···H−C close contacts, are formed in TMGDB and considerably stabilize its folding conformers with $g^{\pm}g^{\mp}$ sequences in the central CH_2−CH_2 bonds. The folding conformers may be sources of dimer fluorescence characteristic of TMGDB and PTT. Configurational properties and thermodynamic quantities of PTT were derived from the refined RIS calculations with the MO energies established for TMGDB. Structures and properties of PTT and poly(ethylene terephthalate) were compared and discussed mainly in terms of their intramolecular attractive interactions.

Introduction

In the 1940s, poly(ethylene terephthalate) (PET) and poly(trimethylene terephthalate) (PTT, Figure 1a) were patented. Immediately, PET was commercialized to be mass-produced for fibers, films, bottles, and engineering plastics, whereas commercial production of PTT had long remained unrealized because of its expensive precursor, 1,3-propanediol (PDO). In the early 1990s, however, continuous hydroformylation of ethylene oxide enabled economic production of PDO. Nowadays, PDO has also been produced via a biological process from corn sugar. With the aid of these technical innovations, commercial manufacturing of PTT was actualized. Compared with PET, PTT has some superior performances such as durability, softness, and permanent stain resistance, thus being used in activewear, carpets, and automotive fabrics.[1]

In a previous paper,[2] we have offered our interpretation of conformational characteristics and configurational properties of PET. Unexpectedly, our results are significantly different from those of previous studies: the structures and properties of PET are substantively influenced by complicated intramolecular attractive interactions. To confirm the conclusions there, this study has dealt with PTT, a homologue of PET; we have conducted ab initio molecular orbital (MO) calculations and NMR experiments for its model compound, trimethylene glycol dibenzoate (TMGDB, Figure 1b), and the refined rotational isomeric state (RIS) calculations for PTT. In the form of a comparative study of PTT and PET, this paper presents our investigations for TMGDB and PTT and new understanding of structures and properties of the aromatic polyesters. To begin with, we would like to emphasize that the only difference between PET and PTT lies in the number (m) of methylene units in the O−$(CH_2)_m$−O part (hereafter referred to as 'spacer' as used for main-chain liquid crystals). Accordingly, all dissimilarities between PET and PTT in structures and properties must be attributed only to whether $m = 2$ or 3.

*To whom correspondence should be addressed. E-mail: sasanuma@faculty.chiba-u.jp. Fax: +81 43 290 3394.

Computations and Experiments

MO Calculations. Density functional and ab initio MO calculations were carried out with the Gaussian03 program[3] installed on an HPC Silent-SCC T2 or an HPC SCC System-L computer. For each conformer of TMGDB, the geometrical parameters were fully optimized at the B3LYP/6-311+G(2d, p) level, and the thermal-correction term to the Gibbs free energy (at 25 °C and 510 K), dipole moment, and polarizability were calculated concomitantly. All self-consistent field (SCF) calculations were conducted under the tight convergence. With the optimized geometry, the SCF energy (SCF (MP2)) was computed at the MP2/6-311+G-(2d, p) level. The Gibbs free energy was evaluated from the SCF (MP2) and thermal-correction energies, being given here as the difference from that of the all-trans conformer and denoted as ΔG_k (k: conformer). The ΔG_k values for benzene environments at 25 °C and 510 K were also calculated at the MP2/6-311+G(2d, p) level with the integral equation formalism of the polarizable continuum model.[4,5] The molecular geometry and thermal correction term for the gas phase were also used for the benzene environments. The MO data on the benzene environment at 510 K are expected to represent molten PTT around this temperature, because the dielectric constant (3.1) of PTT at room temperature[6] is close to that (2.3) of benzene.

Vicinal coupling constants of TMGDB for ^{13}C NMR analyses were calculated at the B3LYP/6-311++G(3df, 3pd)//B3LYP/6-311+G(2d, p) level. Bond lengths, bond

Published on Web 08/12/2009

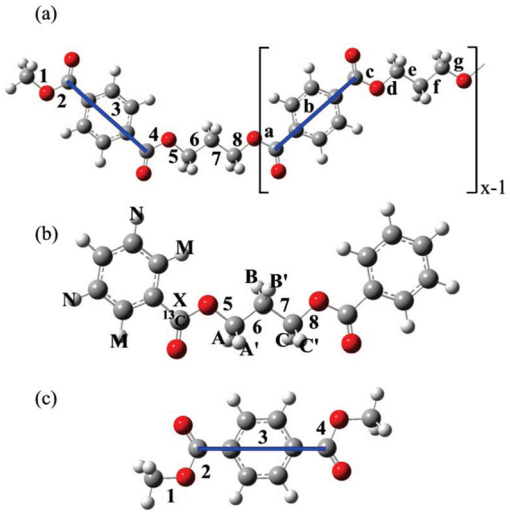

Figure 1. All-trans states of (a) poly(trimethylene terephthalate) (PTT), (b) trimethylene glycol dibenzoate (TMGDB), and (c) dimethyl terephthalate. The thick line segments express virtual bonds of the aromatic rings. The bonds are labeled as indicated. The hydrogen and carbon atoms of TMGDB are partly designated to represent spin systems of NMR spectra shown in Figure 3.

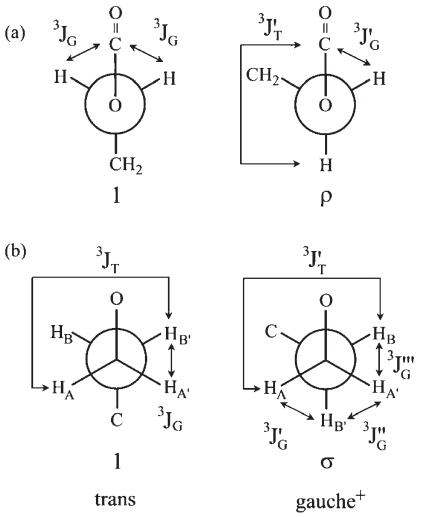

Figure 2. Rotational isomeric states around (a) O−CH_2 and (b) CH_2−CH_2 bonds of the spacers of TMGDB and PTT with definitions of vicinal trans (^3J_T) and gauche (^3J_G) coupling constants. The unity and Greek letters, ρ and σ, represent first-order interactions.

angles, and dihedral angles used in the refined RIS computations for PTT were determined by geometrical optimization at the B3LYP/6-31G(d) level for conformers of trimethyleneglycol bis(dimethyl terephthalate).

Sample Preparation. Trimethylene glycol dibenzoate-$^{13}C_1$ (TMGDB-$^{13}C_1$) was prepared as follows. Benzoyl chloride (0.25 mol) was added dropwise through a dropping funnel to trimethylene glycol (0.30 mol) and anhydrous pyridine (0.25 mol) in a flask equipped with a reflux condenser and a thermometer. The reaction mixture was stirred at room temperature for 11 h and underwent extraction with ether and water. The organic layer was washed three times with 5% aqueous sodium bicarbonate, dried overnight over anhydrous magnesium sulfate, and filtered. The ether was removed in a rotary evaporator, and the residue was distilled under reduced pressure to yield trimethylene glycol monobenzoate (1 mmHg, 140 °C, 10.7 g).

Benzoyl-*carbonyl*-^{13}C chloride (Isotec, 99 atom % ^{13}C, 1 g) was added dropwise to trimethylene glycol monobenzoate (1.9 g) and anhydrous pyridine (0.7 mL). Afterward, the reaction mixture was treated as described above, except for the final purification. The crude product was recrystallized twice from absolute ethanol to yield TMGDB-$^{13}C_1$ (0.66 g). Unlabeled trimethylene glycol dibenzoate was also prepared in the same way.

NMR Measurements. ^{1}H (^{13}C) NMR spectra were recorded at 500 MHz (126 MHz) on a JEOL JNM-LA500 spectrometer equipped with a variable temperature controller in the Chemical Analysis Center of Chiba University. The measurement temperatures were 15, 25, 35, 45, and 55 °C and maintained within ± 0.1 °C fluctuations. Free induction decays were accumulated 32 (256) times. The $\pi/2$ pulse width, data acquisition time, and recycle delay were 5.6 (5.0) μs, 3.3 (2.0) s, and 3.7 (2.0) s, respectively. Here, the values in the parentheses are ^{13}C NMR parameters. The gated decoupling technique was employed in the ^{13}C NMR experiments. The solvents were cyclohexane-d_{12}, benzene-d_6, chloroform-d, methanol-d_4, and dimethyl-d_6 sulfoxide, and the solute concentration was ca. 5 vol %. The NMR spectra were simulated with the gNMR program[7] to derive chemical shifts and coupling constants.

Results and Discussion

^{1}H and ^{13}C NMR of TMGDB and TMGDB-$^{13}C_1$. For methylene protons in the spacer of TMGDB, two vicinal ^{1}H−^{1}H coupling constants determined experimentally, $^3J_{HH}$ ($=^3J_{AB}=^3J_{A'B'}$) and $^3J'_{HH}$($=^3J_{AB'}=^3J_{A'B}$), are related to trans and gauche fractions of the CH_2−CH_2 bond in the spacer:[8]

$$^3J_{HH} = {}^3J_G p_t + \frac{{}^3J'_T + {}^3J''_G}{2} p_g \quad (1)$$

and

$$^3J'_{HH} = {}^3J_T p_t + \frac{{}^3J'_G + {}^3J'''_G}{2} p_g \quad (2)$$

where ^3J_T's and ^3J_G's are defined in Figure 2. The definition of bond conformations leads to

$$p_t + p_g = 1 \quad (3)$$

Figure 2 illustrates that the vicinal ^{13}C−^{1}H coupling constant ($^3J_{CH}$) can be expressed as a function of trans (p_t) and gauche (p_g) fractions of the O−CH_2 bond in the spacer:[8]

$$^3J_{CH} = {}^3J_G p_t + \frac{{}^3J'_T + {}^3J'_G}{2} p_g \quad (4)$$

where $^3J'_T$, ^3J_G, and $^3J'_G$, defined in Figure 2, are vicinal trans and gauche coupling constants, respectively. To derived p_t and p_g values of the CH_2−CH_2 and O−CH_2 bonds from the above equations, ^{1}H and ^{13}C NMR spectra of both TMGDB and TMGDB-$^{13}C_1$ were measured and analyzed.

Shown in parts a and b of Figure 3 are ^{1}H NMR spectra of methylene groups AA′ (CC′) and BB′ of TMGDB, respectively. For the atom designations, see Figure 1b. The AA′ and CC′ parts (Figure 3c) of TMGDB-$^{13}C_1$ appear to be a triplet of triplets, because the asymmetrically ^{13}C-labeled carbonyl carbon (X) renders the two O−CH_2 methylene groups nonequivalent. Figure 3e shows a ^{13}C NMR spectrum observed from the ^{13}C-labeled carbonyl carbon; it exhibits a complicated fine structure due to ^{13}C−^{1}H couplings with the methylene and phenyl protons. The five spectra, measured with the same solvent (benzene-d_6) at 25 °C, are expected to have common ^{1}H−^{1}H and ^{13}C−^{1}H

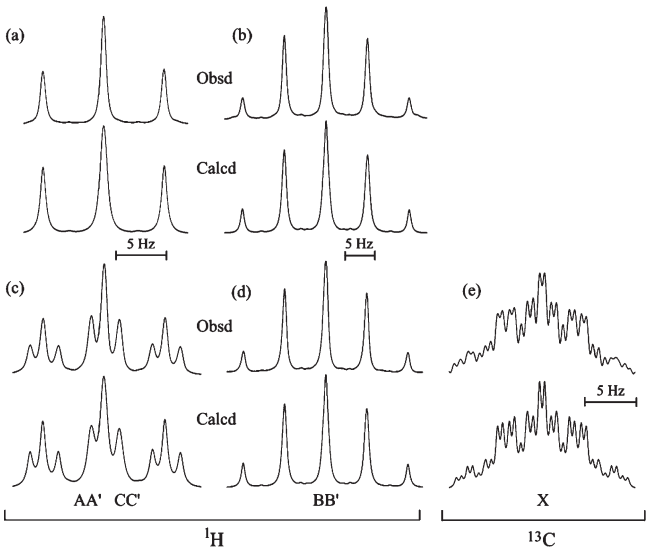

Figure 3. ^{1}H and ^{13}C NMR spectra of TMGDB (a and b) and TMGDB-$^{13}C_1$ (c–e) in benzene-d_6 at 25 °C. For the atom designations, A, A′, B, B′, C, C′, and X, see Figure 1.

coupling constants. On this assumption, the spectra were satisfactorily simulated as shown in Figure 3, and the coupling constants were optimized: $^3J_{HH}$ = 7.15, $^3J'_{HH}$= 5.45, $^3J_{CH}$ = 2.90, $^3J_{XM}$ = 4.10, and $^4J_{XN}$ = 1.09 Hz. The $^3J_{HH}$, $^3J'_{HH}$, and $^3J_{CH}$ values for all the solutions, determined in the same way, are listed in Table 1.

According to eqs 1–3, bond conformations of the CH_2–CH_2 bond in the spacer were evaluated from the $^3J_{HH}$ and $^3J'_{HH}$ values. Then, the coefficients (^3J_T's and ^3J_G's) in eqs 1 and 2 were taken from those of 2-substituted 1,3-dioxanes (set A)[9] and 1,3-dioxane in CS_2 at −90 °C (set B),[10] because these cyclic ethers have the same O–CH_2–CH_2–CH_2–O bond sequence as TMGDB and cease flip-flopping. For the individual ^3J_T and ^3J_G values employed, see the footnote of Table 2. The p_t and p_g values calculated from eqs 1 and 2 were divided by their sum to satisfy eq 3. The trans fractions thus obtained are listed in Table 2. In the analysis for $^3J_{CH}$ with eqs 3 and 4, the three coefficients, ^3J_T, ^3J_G, and $^3J'_G$, were derived from (set a) a Karplus equation for the C–O–C–H bond sequence: $^3J_{COCH} = 5.7\cos^2\phi + 0.6\cos\phi + 0.5$ (ϕ: dihedral angle between ^{13}C and ^{1}H).[11] Then, the ϕ values were set equal to those optimized for TMGDB at the B3LYP/6-311+G(2d, p) level. In addition, the three ^3J coefficients obtained from (set b) MO calculations at the B3LYP/6-311++G(3df, 3pd)//B3LYP/6-311+G(2d, p) level for TMGDB itself were used (see the footnote of Table 2). For the CH_2–CH_2 bond of TMGDB, the p_t values are found within a narrow range of 0.11–0.15; the gauche states are strongly stabilized. On the other hand, the O–CH_2 bond shows a moderate trans preference. As for the solvents employed here, both p_t values little depend on medium polarity.

MO Calculations and Conformational Energies. Owing to the coplanar structure of phenyl and ester groups of TMGDB, only bonds 5, 6, 7, and 8 (see Figure 1) are rotatable. Under the RIS approximation,[12,13] three states, t, g^+, and g^-, are defined for these four bonds; thus, the spacer has 81 conformations. However, its molecular symmetry reduces the number of independent conformers to 25. Table 3 shows free energies (ΔG_k's) of the 25 conformers. In the geometrical optimization, five conformers of k = 10, 21, 22, 24, and 25 did not reach their stationary points on the potential energy surface; therefore, these five states are excluded from conformer ensembles of TMGDB and PTT in the following treatments. Here, for example, the notation $tg^+g^-g^+$ represents that bonds 5, 6, 7, and 8 adopt t, g^+, g^-, and g^+ conformations, respectively.

Table 1. Observed Vicinal ^{1}H–^{1}H and ^{13}C–^{1}H Coupling Constants of TMGDB and TMGDB-$^{13}C_1$[a]

solvent	dielectric constant[b]	temp, °C	$^3J_{HH}$	$^3J'_{HH}$	$^3J_{CH}$
cyclohexane-d_{12}	2.0	15	7.05	5.38	2.95
		25	7.05	5.43	2.98
		35	7.04	5.46	3.04
		45	7.00	5.56	3.04
		55	6.97	5.61	3.05
benzene-d_6	2.3	15	7.15	5.42	2.86
		25	7.15	5.45	2.90
		35	7.14	5.48	2.93
		45	7.13	5.51	2.94
		55	7.12	5.53	2.97
chloroform-d	4.8	15	7.09	5.37	2.74
		25	7.08	5.40	2.79
		35	7.08	5.43	2.84
		45	7.06	5.47	2.88
		55	7.06	5.50	2.90
methanol-d_4	32.7	15	7.03	5.31	2.92
		25	7.01	5.34	2.92
		35	6.98	5.36	2.96
		45	6.96	5.40	2.97
		55	6.95	5.43	3.03
dimethyl-d_6 sulfoxide	46.7	15	7.14	5.24	2.82
		25	7.13	5.30	2.87
		35	7.10	5.35	2.87
		45	7.09	5.38	2.89
		55	7.08	5.39	2.94

[a] In Hz. [b] At room temperature.

In Table 3, the ΔG_k values of TMGDB in benzene at the MP2/6-311+G(2d, p) and HF/6-311+G(2d, p) levels are compared. None of the 20 conformers shows any negative ΔG_k (HF) energy, whereas a number of conformers have large negative ΔG_k (MP2) values. It has been well established that the MP2 energy is always more reliable than the HF one. Inasmuch as the MP2 energy differs from HF by electron correlation effects, we may define the electron correlation factor (δG_k) of conformer k as

$$\delta G_k \equiv \Delta G_k(\mathrm{MP2}) - \Delta G_k(\mathrm{HF}) \tag{5}$$

A negative δG_k value is probably ascribed to attractive interaction(s), for example, what is generally called the dispersion force. We can find that tg^+g^-t (k = 11), $tg^+g^-g^+$ (12), $tg^+g^-g^-$ (13), and $g^+g^+g^-g^-$ (23) conformers with pentane-effect-like $g^\pm g^\mp$ folds[12] at the center of the spacer are most unstable in ΔG_k(HF) but most stable in ΔG_k(MP2). The large discrepancies will be discussed later.

The p_t values of TMGDB (Table 2), calculated from ΔG_k (MP)'s for the gas phase and benzene solution are compared with those derived from the above NMR analyses; the MO calculations agree with the NMR data. According to our previous study on PET,[2] higher-order interaction energies of TMGDB have been evaluated as follows. On the assumption that ΔG_k (MP2) values of $tttg^+$ (k = 2) and ttg^+t (3) conformers, respectively, correspond to first-order interaction energies (E_ρ and E_σ) for the O–CH_2 and CH_2–CH_2 bonds, the higher-order interaction energy, E_{α_k}, of conformer k was calculated from

$$E_{\alpha_k} = \Delta G_k - n_{\rho_k}E_\rho - n_{\sigma_k}E_\sigma \tag{6}$$

where n_{ρ_k} and n_{σ_k} are numbers of gauche conformations in the O–CH_2 and CH_2–CH_2 bonds of conformer k, respectively. Therefore, the E_{α_k} parameter may be considered to include all higher-order interactions related to conformer k.

Table 2. Trans Fractions (p_t's) in O−CH_2−CH_2−CH_2−O Bond Sequence of TMGDB

		p_t			
		CH_2-CH_2		O−CH_2	
medium	temp (°C)	set A[a]	set B[b]	set a[c]	set b[d]
		NMR Experiment			
cyclohexane	15	0.12	0.13	0.58	0.51
	25	0.13	0.14	0.57	0.50
	35	0.13	0.14	0.55	0.48
	45	0.14	0.15	0.55	0.48
	55	0.15	0.15	0.54	0.48
benzene	15	0.12	0.13	0.61	0.53
	25	0.12	0.13	0.59	0.52
	35	0.13	0.14	0.58	0.51
	45	0.13	0.14	0.58	0.51
	55	0.13	0.14	0.57	0.50
chloroform	15	0.12	0.13	0.65	0.56
	25	0.12	0.13	0.63	0.55
	35	0.13	0.13	0.61	0.54
	45	0.13	0.14	0.60	0.53
	55	0.13	0.14	0.59	0.52
methanol	15	0.12	0.13	0.59	0.52
	25	0.12	0.13	0.59	0.52
	35	0.13	0.14	0.57	0.50
	45	0.13	0.14	0.57	0.50
	55	0.13	0.14	0.55	0.49
dimethyl sulfoxide	15	0.11	0.12	0.62	0.54
	25	0.11	0.12	0.60	0.53
	35	0.12	0.13	0.60	0.53
	45	0.12	0.13	0.60	0.52
	55	0.12	0.13	0.58	0.51
		MO Calculated[e]			
gas phase	15	0.10		0.51	
	25	0.10		0.51	
	35	0.11		0.51	
	45	0.12		0.51	
	55	0.12		0.51	
benzene	15	0.11		0.52	
	25	0.11		0.52	
	35	0.12		0.52	
	45	0.13		0.52	
	55	0.13		0.52	

[a] ${}^3J_T' = 12.4$, ${}^3J_G' = 2.6$, ${}^3J_G'' = 1.3$, and ${}^3J_G''' = 5.0$ Hz (from 2-substituted 1,3-dioxanes, ref 9). The ${}^3J_T$ and ${}^3J_G$ values were obtained from ${}^3J_T = {}^3J_T'$ and ${}^3J_G = ({}^3J_G' + {}^3J_G'' + {}^3J_G''')/3$. [b] ${}^3J_T' = 12.3$, ${}^3J_G' = 2.3$, ${}^3J_G'' = 1.2$, and ${}^3J_G''' = 4.9$ Hz (from 1,3-dioxane, ref 10). It was also assumed that ${}^3J_T = {}^3J_T'$ and ${}^3J_G = ({}^3J_G' + {}^3J_G'' + {}^3J_G''')/3$. [c] ${}^3J_G = 1.7$ Hz ($\phi = 121.5°$), ${}^3J_T' = 5.4$ Hz ($\phi = 28.6°$), and ${}^3J_G' = 3.9$ Hz ($\phi = 145.4°$). (from the Karplus equation, ref 11). [d] ${}^3J_G = 1.10$, ${}^3J_T' = 6.29$, and ${}^3J_G' = 3.41$ Hz (MO calculations for TMGDB at the B3LYP/6-311++G(3df, 3pd) level, this study). [e] At the MP2/6-311+G(2d, p)//B3LYP/6-311+G(2d, p) level.

The conformer free energies were divided into two first-order (E_ρ and E_σ) and 22 higher-order (E_{α_k}, $k = 4-25$) interaction energies (Table 4). The E_{α_k} values of the five nonexistent conformers of $k = 10$, 21, 22, 24, and 25 are expressed by ∞.

To apply the MO free energies as they are to the RIS calculations, this study has adopted the above E_ρ, E_σ, and E_{α_k} energies and the following statistical weight matrices (U_j's, j: bond number, see Figure 1) for the spacer:

$$U_5 = \begin{bmatrix} 1 \\ 0 \\ 0 \end{bmatrix} \otimes [1 \quad \rho \quad \rho] \tag{7}$$

$$U_6 = I_3 \otimes [1 \quad \sigma \quad \sigma] \tag{8}$$

$$U_7 = I_3 \otimes I_3 \otimes [1 \quad \sigma \quad \sigma] \tag{9}$$

Table 3. Conformer Free Energies (ΔG_k's) of TMGDB, Evaluated by Ab Initio MO Calculations

						ΔG_k[a]				δG_k[b]
						gas	benzene			benzene
						MP2[c]	MP2[c]		HF[d]	
k	conformation				M_k[e]	25 °C	25 °C	510 K	25 °C	25 °C
1	t	t	t	t	1	0.00	0.00	0.00	0.00	0.00
2	t	t	t	g^+	4	0.76	0.85	1.42	1.60	−0.75
3	t	t	g^+	t	4	−0.65	−0.56	−0.25	0.07	−0.63
4	t	t	g^+	g^+	4	−0.54	−0.38	−0.07	0.87	−1.25
5	t	t	g^+	g^-	4	−0.72	−0.55	−0.79	1.12	−1.67
6	t	g^+	t	g^+	4	−0.94	−0.63	−0.38	0.83	−1.46
7	t	g^+	t	g^-	4	−0.81	−0.56	−0.22	0.81	−1.37
8	t	g^+	g^+	t	2	−1.18	−0.98	−0.33	0.38	−1.36
9	t	g^+	g^+	g^+	4	−1.32	−0.99	−0.42	0.98	−1.97
10	t	g^+	g^+	g^-	4			(absent)[f]		
11	t	g^+	g^-	t	2	−1.06	−0.89	−0.23	2.57	−3.46
12	t	g^+	g^-	g^+	4	−1.92	−1.61	−0.66	3.87	−5.48
13	t	g^+	g^-	g^-	4	−2.24	−1.97	−1.66	2.28	−4.25
14	g^+	t	t	g^+	2	0.84	1.03	1.74	2.52	−1.49
15	g^+	t	t	g^-	2	1.01	1.13	1.45	2.68	−1.55
16	g^+	t	g^+	g^+	4	0.20	0.45	1.00	2.59	−2.14
17	g^+	t	g^+	g^-	4	−0.11	0.24	0.81	2.77	−2.53
18	g^+	t	g^-	g^+	4	0.06	0.40	1.11	2.78	−2.38
19	g^+	t	g^-	g^-	4	0.02	0.31	1.10	2.23	−1.92
20	g^+	g^+	g^+	g^+	2	−0.75	−0.33	0.54	2.22	−2.55
21	g^+	g^+	g^+	g^-	4			(absent)[f]		
22	g^+	g^+	g^-	g^+	4			(absent)[f]		
23	g^+	g^+	g^-	g^-	2	−0.76	−0.47	0.44	4.42	−4.89
24	g^+	g^-	g^+	g^-	2			(absent)[f]		
25	g^+	g^-	g^-	g^+	2			(absent)[f]		

[a] In kcal mol^{-1}. [b] In kcal mol^{-1}. $\delta G_k = \Delta G_k(\text{MP2}) - \Delta G_k(\text{HF})$. [c] At the MP2/6-311+G(2d, p)//B3LYP/6-311+G(2d, p) level. [d] At the HF/6-311+G(2d, p)//B3LYP/6-311+G(2d, p) level. [e] Multiplicity. [f] The local minimum of the potential was not found by the geometrical optimization.

and

$$U_8 = U_8^{\text{higher}} U_8^{\text{1st}} \tag{10}$$

where the symbol ⊗ stands for direct product, I_3 is the identity matrix of size 3, $U_8{}^{\text{1st}}$ is the factor for the first-order interaction around bond 8,

$$U_8^{\text{1st}} = I_3 \otimes I_3 \otimes \begin{bmatrix} 1 & 0 & 0 \\ 0 & \rho & 0 \\ 0 & 0 & \rho \end{bmatrix} \tag{11}$$

and $U_8{}^{\text{higher}}$ is that for the higher-order interactions (shown in Figure 4). The statistical weights are calculated from the corresponding conformational energies according to, for example, $\alpha_k = \exp(-E_{\alpha_k}/RT)$, where R is the gas constant, and T is the absolute temperature.

Molar Kerr Constant. Mendicuti et al.[14] measured the dipole moment of TMGDB dissolved in benzene at 25 °C and the molar Kerr constant of its cyclohexane solution at 25 °C. We attempted to reproduce the experimental dipole moment and molar Kerr constant of TMGDB from the conformer free energies, dipole moments, and polarizabilities that our MO calculations yielded.

The molar Kerr constant ${}_mK$ is expressed as[15]

$${}_mK = \frac{2\pi N_A}{15 k_B T}\left[\frac{\mu^T \hat{\alpha} \mu}{k_B T} + \text{tr}(\hat{\alpha}\hat{\alpha})\right] \tag{12}$$

where N_A is Avogadro's number, k_B is Boltzmann's constant, and μ^T is the transpose of dipole moment μ, that is, $\mu^T = (\mu_x, \mu_y, \mu_z)$. Here, x, y, and z are the principal axes of

polarizability. The anisotropic part $\hat{\alpha}$ of the polarizability tensor α is given by

$$\hat{\alpha} = \alpha - \frac{1}{3}\mathrm{tr}(\alpha)I_3 \tag{13}$$

Table 4. Conformational Energies of TMGDB and PTT, Evaluated by ab Initio MO Calculations

	conformational energy[a] (kcal mol^{-1})		
	gas	benzene	
interaction	25 °C	25 °C	510 K
	First-Order		
ρ	0.76	0.85	1.42
σ	−0.65	−0.56	−0.25
γ^b	0.16	0.15	0.16
	Higher-Order		
α_4	−0.65	−0.67	−1.24
α_5	−0.83	−0.84	−1.96
α_6	−1.05	−0.92	−1.55
α_7	−0.92	−0.85	−1.39
α_8	0.12	0.14	0.17
α_9	−0.78	−0.72	−1.34
α_{10}	∞	∞	∞
α_{11}	0.24	0.23	0.27
α_{12}	−1.38	−1.34	−1.58
α_{13}	−1.70	−1.70	−2.58
α_{14}	−0.68	−0.67	−1.10
α_{15}	−0.51	−0.57	−1.39
α_{16}	−0.67	−0.69	−1.59
α_{17}	−0.98	−0.90	−1.78
α_{18}	−0.81	−0.74	−1.48
α_{19}	−0.85	−0.83	−1.49
α_{20}	−0.97	−0.91	−1.80
α_{21}	∞	∞	∞
α_{22}	∞	∞	∞
α_{23}	−0.98	−1.05	−1.90
α_{24}	∞	∞	∞
α_{25}	∞	∞	∞

[a] At the MP2/6-311+G(2d, p)//B3LYP/6-311+G(2d, p) level. [b] The cis−trans energy difference around the virtual bond, evaluated from dimethyl terephthalate (Figure 1c). See ref 2.

where

$$\alpha = \mathrm{diag}(\alpha_x, \alpha_y, \alpha_z) \tag{14}$$

The observed molar Kerr constant $\langle {}_{\mathrm{m}}K\rangle$ is related to conformer free energies according to

$$\langle {}_{\mathrm{m}}K\rangle = \sum_k {}_{\mathrm{m}}K_k M_k \exp\left(-\frac{\Delta G_k}{RT}\right) \Big/ \sum_k M_k \exp\left(-\frac{\Delta G_k}{RT}\right) \tag{15}$$

where ${}_{\mathrm{m}}K_k$ and M_k are the molar Kerr constant and multiplicity of conformer k, respectively. The average dipole moment is similarly derived from

$$\langle \mu\rangle = \sum_k \mu_k M_k \exp\left(-\frac{\Delta G_k}{RT}\right) \Big/ \sum_k M_k \exp\left(-\frac{\Delta G_k}{RT}\right) \tag{16}$$

where μ_k is the dipole moment of conformer k.

The Gaussian03 program[3] provides both dipole moment vector and polarizability tensor with respect to the so-called standard orientation (X, Y, and Z); the origin is located at the center of nuclear charges, and the axes are set on the basis of molecular symmetry. In symmetric conformers such as tttt ($k = 1$), tg$^+$g$^+$t (8), g$^+$ttg$^+$ (14), and g$^+$g$^+$g$^+$g$^+$ (20) of TMGDB, the x, y, and z axes agree with the X, Y, and Z ones. Even in the others, off-diagonal elements of the polarizability tensors are fully close to zero, and hence the tensors are nearly diagonalized (see Tables S1 and S2, Supporting Information). Accordingly, the dipole moments and polarizabilities obtained from the MO calculations atthe B3LYP/6-311+G(2d, p) level were employed as they are under conditions of $\mu_x = \mu_X$, $\mu_y = \mu_Y$, $\mu_z = \mu_Z$, $\alpha_x = \alpha_{XX}$, $\alpha_y = \alpha_{YY}$, and $\alpha_z = \alpha_{ZZ}$. Substitution of the μvectors (Table S1), α tensors (Table S2), and ΔG_k (MP2) energies (benzene, 25 °C, Table 3) into eqs 12−16 yielded $\langle {}_{\mathrm{m}}K\rangle = 7.04 \times 10^{-25}$ m^5 V^{-2} mol^{-1} and $\langle \mu\rangle = 2.59$ D. These results exactly agree with

$$U_8^{\mathrm{higher}} = \begin{array}{c} \\ \mathrm{t\,t\,t} \\ \mathrm{t\,t\,g^+} \\ \mathrm{t\,t\,g^-} \\ \mathrm{t\,g^+t} \\ \mathrm{t\,g^+g^+} \\ \mathrm{t\,g^+g^-} \\ \mathrm{t\,g^-t} \\ \mathrm{t\,g^-g^+} \\ \mathrm{t\,g^-g^-} \\ \mathrm{g^+t\,t} \\ \mathrm{g^+t\,g^+} \\ \mathrm{g^+t\,g^-} \\ \mathrm{g^+g^+t} \\ \mathrm{g^+g^+g^+} \\ \mathrm{g^+g^+g^-} \\ \mathrm{g^+g^-t} \\ \mathrm{g^+g^-g^+} \\ \mathrm{g^+g^-g^-} \\ \mathrm{g^-t\,t} \\ \mathrm{g^-t\,g^+} \\ \mathrm{g^-t\,g^-} \\ \mathrm{g^-g^+t} \\ \mathrm{g^-g^+g^+} \\ \mathrm{g^-g^+g^-} \\ \mathrm{g^-g^-t} \\ \mathrm{g^-g^-g^+} \\ \mathrm{g^-g^-g^-} \end{array} \begin{array}{c} \begin{array}{ccccccccccccccccccccccccccc} \mathrm{t} & \mathrm{g^+} & \mathrm{g^-} & \mathrm{t} & \mathrm{g^+} & \mathrm{g^-} & \mathrm{t} & \mathrm{g^+} & \mathrm{g^-} & \mathrm{t} & \mathrm{g^+} & \mathrm{g^-} & \mathrm{t} & \mathrm{g^+} & \mathrm{g^-} & \mathrm{t} & \mathrm{g^+} & \mathrm{g^-} & \mathrm{t} & \mathrm{g^+} & \mathrm{g^-} & \mathrm{t} & \mathrm{g^+} & \mathrm{g^-} & \mathrm{t} & \mathrm{g^+} & \mathrm{g^-} \end{array} \\ \begin{pmatrix} \alpha_1 & \alpha_2 & \alpha_2 & 0 & 0 & 0 & 0 & 0 & 0 & 0 & 0 & 0 & 0 & 0 & 0 & 0 & 0 & 0 & 0 & 0 & 0 & 0 & 0 & 0 & 0 & 0 & 0 \\ 0 & 0 & 0 & \alpha_3 & \alpha_4 & \alpha_5 & 0 & 0 & 0 & 0 & 0 & 0 & 0 & 0 & 0 & 0 & 0 & 0 & 0 & 0 & 0 & 0 & 0 & 0 & 0 & 0 & 0 \\ 0 & 0 & 0 & 0 & 0 & 0 & \alpha_3 & \alpha_5 & \alpha_4 & 0 & 0 & 0 & 0 & 0 & 0 & 0 & 0 & 0 & 0 & 0 & 0 & 0 & 0 & 0 & 0 & 0 & 0 \\ 0 & 0 & 0 & 0 & 0 & 0 & 0 & 0 & 0 & \alpha_3 & \alpha_6 & \alpha_7 & 0 & 0 & 0 & 0 & 0 & 0 & 0 & 0 & 0 & 0 & 0 & 0 & 0 & 0 & 0 \\ 0 & 0 & 0 & 0 & 0 & 0 & 0 & 0 & 0 & 0 & 0 & 0 & \alpha_8 & \alpha_9 & \alpha_{10} & 0 & 0 & 0 & 0 & 0 & 0 & 0 & 0 & 0 & 0 & 0 & 0 \\ 0 & 0 & 0 & 0 & 0 & 0 & 0 & 0 & 0 & 0 & 0 & 0 & 0 & 0 & 0 & \alpha_{11} & \alpha_{12} & \alpha_{13} & 0 & 0 & 0 & 0 & 0 & 0 & 0 & 0 & 0 \\ 0 & 0 & 0 & 0 & 0 & 0 & 0 & 0 & 0 & 0 & 0 & 0 & 0 & 0 & 0 & 0 & 0 & 0 & \alpha_3 & \alpha_7 & \alpha_6 & 0 & 0 & 0 & 0 & 0 & 0 \\ 0 & 0 & 0 & 0 & 0 & 0 & 0 & 0 & 0 & 0 & 0 & 0 & 0 & 0 & 0 & 0 & 0 & 0 & 0 & 0 & 0 & \alpha_{11} & \alpha_{13} & \alpha_{12} & 0 & 0 & 0 \\ 0 & 0 & 0 & 0 & 0 & 0 & 0 & 0 & 0 & 0 & 0 & 0 & 0 & 0 & 0 & 0 & 0 & 0 & 0 & 0 & 0 & 0 & 0 & 0 & \alpha_8 & \alpha_{10} & \alpha_9 \\ \alpha_2 & \alpha_{14} & \alpha_{15} & 0 & 0 & 0 & 0 & 0 & 0 & 0 & 0 & 0 & 0 & 0 & 0 & 0 & 0 & 0 & 0 & 0 & 0 & 0 & 0 & 0 & 0 & 0 & 0 \\ 0 & 0 & 0 & \alpha_6 & \alpha_{16} & \alpha_{17} & 0 & 0 & 0 & 0 & 0 & 0 & 0 & 0 & 0 & 0 & 0 & 0 & 0 & 0 & 0 & 0 & 0 & 0 & 0 & 0 & 0 \\ 0 & 0 & 0 & 0 & 0 & 0 & \alpha_7 & \alpha_{18} & \alpha_{19} & 0 & 0 & 0 & 0 & 0 & 0 & 0 & 0 & 0 & 0 & 0 & 0 & 0 & 0 & 0 & 0 & 0 & 0 \\ 0 & 0 & 0 & 0 & 0 & 0 & 0 & 0 & 0 & \alpha_4 & \alpha_{16} & \alpha_{19} & 0 & 0 & 0 & 0 & 0 & 0 & 0 & 0 & 0 & 0 & 0 & 0 & 0 & 0 & 0 \\ 0 & 0 & 0 & 0 & 0 & 0 & 0 & 0 & 0 & 0 & 0 & 0 & \alpha_9 & \alpha_{20} & \alpha_{21} & 0 & 0 & 0 & 0 & 0 & 0 & 0 & 0 & 0 & 0 & 0 & 0 \\ 0 & 0 & 0 & 0 & 0 & 0 & 0 & 0 & 0 & 0 & 0 & 0 & 0 & 0 & 0 & \alpha_{13} & \alpha_{22} & \alpha_{23} & 0 & 0 & 0 & 0 & 0 & 0 & 0 & 0 & 0 \\ 0 & 0 & 0 & 0 & 0 & 0 & 0 & 0 & 0 & 0 & 0 & 0 & 0 & 0 & 0 & 0 & 0 & 0 & \alpha_5 & \alpha_{18} & \alpha_{17} & 0 & 0 & 0 & 0 & 0 & 0 \\ 0 & 0 & 0 & 0 & 0 & 0 & 0 & 0 & 0 & 0 & 0 & 0 & 0 & 0 & 0 & 0 & 0 & 0 & 0 & 0 & 0 & \alpha_{12} & \alpha_{22} & \alpha_{24} & 0 & 0 & 0 \\ 0 & 0 & 0 & 0 & 0 & 0 & 0 & 0 & 0 & 0 & 0 & 0 & 0 & 0 & 0 & 0 & 0 & 0 & 0 & 0 & 0 & 0 & 0 & 0 & \alpha_{10} & \alpha_{25} & \alpha_{21} \\ \alpha_2 & \alpha_{15} & \alpha_{14} & 0 & 0 & 0 & 0 & 0 & 0 & 0 & 0 & 0 & 0 & 0 & 0 & 0 & 0 & 0 & 0 & 0 & 0 & 0 & 0 & 0 & 0 & 0 & 0 \\ 0 & 0 & 0 & \alpha_7 & \alpha_{19} & \alpha_{18} & 0 & 0 & 0 & 0 & 0 & 0 & 0 & 0 & 0 & 0 & 0 & 0 & 0 & 0 & 0 & 0 & 0 & 0 & 0 & 0 & 0 \\ 0 & 0 & 0 & 0 & 0 & 0 & \alpha_6 & \alpha_{17} & \alpha_{16} & 0 & 0 & 0 & 0 & 0 & 0 & 0 & 0 & 0 & 0 & 0 & 0 & 0 & 0 & 0 & 0 & 0 & 0 \\ 0 & 0 & 0 & 0 & 0 & 0 & 0 & 0 & 0 & \alpha_5 & \alpha_{17} & \alpha_{18} & 0 & 0 & 0 & 0 & 0 & 0 & 0 & 0 & 0 & 0 & 0 & 0 & 0 & 0 & 0 \\ 0 & 0 & 0 & 0 & 0 & 0 & 0 & 0 & 0 & 0 & 0 & 0 & \alpha_{10} & \alpha_{21} & \alpha_{25} & 0 & 0 & 0 & 0 & 0 & 0 & 0 & 0 & 0 & 0 & 0 & 0 \\ 0 & 0 & 0 & 0 & 0 & 0 & 0 & 0 & 0 & 0 & 0 & 0 & 0 & 0 & 0 & \alpha_{12} & \alpha_{24} & \alpha_{22} & 0 & 0 & 0 & 0 & 0 & 0 & 0 & 0 & 0 \\ 0 & 0 & 0 & 0 & 0 & 0 & 0 & 0 & 0 & 0 & 0 & 0 & 0 & 0 & 0 & 0 & 0 & 0 & \alpha_4 & \alpha_{19} & \alpha_{16} & 0 & 0 & 0 & 0 & 0 & 0 \\ 0 & 0 & 0 & 0 & 0 & 0 & 0 & 0 & 0 & 0 & 0 & 0 & 0 & 0 & 0 & 0 & 0 & 0 & 0 & 0 & 0 & \alpha_{13} & \alpha_{23} & \alpha_{22} & 0 & 0 & 0 \\ 0 & 0 & 0 & 0 & 0 & 0 & 0 & 0 & 0 & 0 & 0 & 0 & 0 & 0 & 0 & 0 & 0 & 0 & 0 & 0 & 0 & 0 & 0 & 0 & \alpha_9 & \alpha_{21} & \alpha_{20} \end{pmatrix} \end{array}$$

Figure 4. Higher-order interaction factor (U_8^{higher}) of the statistical weight matrix of bonds 8 and g of TMGDB and PTT. The rows and columns are assigned to rotational states of the previous and current bonds, respectively. For example, the label on the sixth row, tg$^+$g$^-$ indicates that bonds 5 (d), 6 (e), and 7 (f) adopt t, g$^+$, and g$^-$ conformations, respectively.

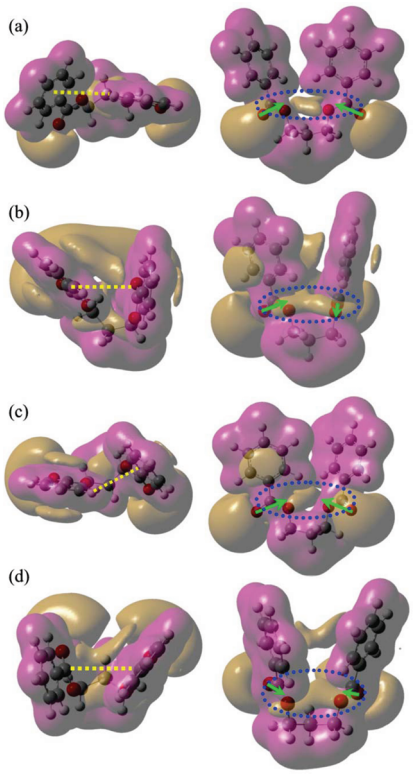

Figure 5. Electrostatic potential distributions of four folding conformers, (a) tg^+g^-t, (b) $tg^+g^-g^+$, (c) $tg^+g^-g^-$, and (d) $g^+g^+g^-g^-$, stabilized considerably by intramolecular attractive interactions: top (left) and side (right) views. The dashed lines, dotted circles, and arrows represent $\pi-\pi$ interactions of the terephthaloyl rings, electrostatic attractions between the ester groups, and dipole moments of the ester groups, respectively.

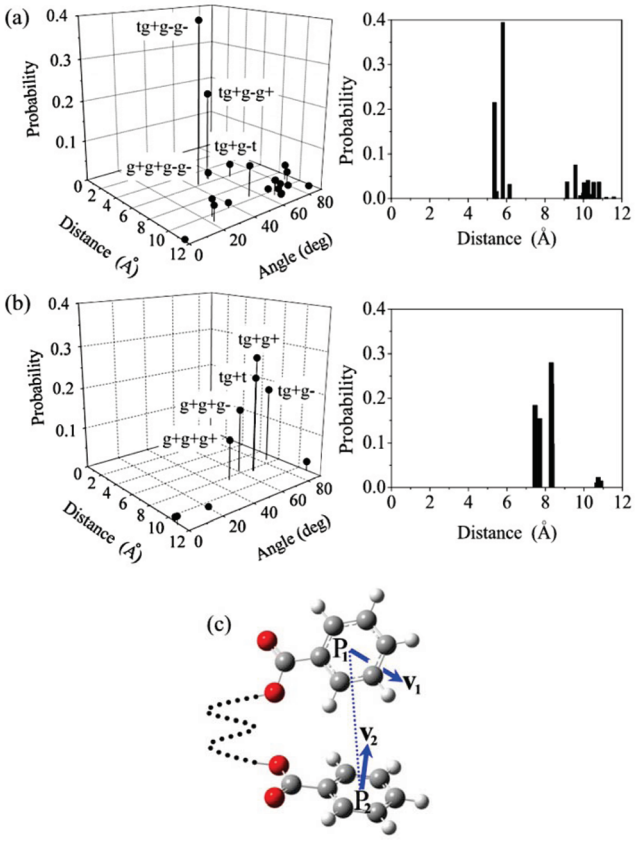

Figure 6. Existing probabilities of conformers of (a) TMGDB and (b) ethylene glycol dibenzoate (EGDB), a model compound of PET, as a function of the distance ($\overline{P_1P_2}$) and angle ($\angle \mathbf{v}_1 \wedge \mathbf{v}_2$) between phenyl rings (left). The distance distributions are separately drawn (right).

the experimental values,[14] $\langle {}_mK \rangle = 6.9 \pm 3.9 \times 10^{-25}$ m^5 V^{-2} mol^{-1} and $\langle \mu^2 \rangle^{1/2} = 2.59$ D.

As shown above, the MO calculations fully reproduced both NMR and electric birefringence experiments for TMGDB. Therefore, we are allowed to discuss intramolecular interactions formed in TMGDB and PTT and conformational characteristics and configurational properties of unperturbed PTT chains from the ΔG_k (MP2) and conformational energies established as above.

Intramolecular Interactions of TMGDB. As described above, the electron correlation factor, δG_k, is due to intramolecular attractive interactions. The above four folding conformers in particular have large negative δG_k values: tg^+g^-t ($k=11$, $\delta G_k = -3.46$ kcal mol^{-1}), $tg^+g^-g^+$ ($k=12$, $\delta G_k = -5.48$ kcal mol^{-1}), $tg^+g^-g^-$ ($k=13$, $\delta G_k = -4.25$ kcal mol^{-1}), and $g^+g^+g^-g^-$ ($k=23$, $\delta G_k = -4.89$ kcal mol^{-1}). Figure 5 depicts their structures and electrostatic potentials. The two phenyl groups are close to each other, and part of the π electrons seem to merge together. This phenomenon, termed $\pi-\pi$ interaction, is an attractive interaction. Their phenyl−phenyl distances ($\overline{P_1P_2}$) and angles between $\mathbf{v}_1$ and $\mathbf{v}_2$ vectors ($\angle \mathbf{v}_1 \wedge \mathbf{v}_2$, see Figure 6c) are, respectively, (a) 6.16 Å and 64.2° ($k=11$), (b) 5.37 Å and 52.4° ($k=12$), (c) 5.81 Å and 43.4° ($k=13$), and (d) 5.49 Å and 52.5° ($k=23$). It has been suggested that the $\pi-\pi$ interaction between benzenes is maximized to be −3 to −4 kcal mol^{-1} at $\overline{P_1P_2} = 3.5$ Å and $\mathbf{v}_1 \| \mathbf{v}_2$ or −3 kcal mol^{-1} at $\overline{P_1P_2} = 5.0$ Å and $\mathbf{v}_1 \perp \mathbf{v}_2$.[16] The natural population analysis for the four conformers estimated that partial charges of the carbonyl carbon and $-O-CH_2$ oxygen are +0.99 and −0.67, respectively; some electrostatic attractions may further stabilize these folding structures. As illustrated in Figure 5, dipole−dipole interactions also appear between the ester groups. As found for ethylene glycol dibenzoate (EGDB), a model compound of PET,[2] a number of conformers of TMGDB show C=O···H−C and C−O···H−C close contacts (not depicted here), of which O···H distances are shorter than the sum (2.7 Å) of van der Waals radii of oxygen and hydrogen. In actual fact, intramolecular interactions of the individual conformers may be difficult to divide into such well-defined factors. It has been generally believed that the $g^{\pm}g^{\mp}$ conformations in two successive CH_2-CH_2 bonds give rise to a strong repulsion.[12] For TMGDB, however, the bent conformations allow the two benzoyloxy groups to approach and attract each other, whereas EGDB and PET can hardly form such attractions because of their short spacers.

Intramolecular Dimer Formation. Mattice et al.[17,18] have extensively investigated dimer emission of aromatic polyesters $[-OCC_6H_4COO(CH_2)_mO-]_x$ ($m = 2-6$) and their model compounds $C_6H_5COO(CH_2)_mOOCC_6H_5$ and found that PTT and TMGDB ($m=3$) and PET and EGDB ($m=2$), respectively, yield the largest and smallest intensity ratios (I_D/I_M's) of dimer (wavelength = 390 nm) to monomer (324 nm) emission. Here, we would like to discuss the I_D/I_M ratios of TMGDB (PTT) and EGDB (PET) on the basis of the RIS scheme. Strictly, the system treated here, absorbing and releasing photon energies, would be out of thermodynamic equilibrium. However, the monomer ensemble would obey the Boltzmann distribution provided that the dimers are rarely formed. Whether the fluorescent emission of wavelength ~ 390 nm from PTT and PET is due to a ground-state

Table 5. Configurational Properties, Bond Conformations, Thermodynamic Quantities of Fusion, and Average Geometrical Parameters of PTT, Evaluated from Refined RIS Calculations[a]

		PTT			PET[b]	
		25 °C	510 K[c]	525 K[c]	25 °C	553 K[c]
$\langle r^2\rangle_0/nl^2$ for $x \to \infty$		1.37	2.43	2.47	2.63	2.87
$10^3 d(\ln\langle r^2\rangle_0)/dT$, K^{-1}		3.2	1.1	1.0	0.27	0.41
trans fraction (p_t)	bond a	1.00	1.00	1.00		
	bond b	0.56	0.54	0.54		
	bond c	1.00	1.00	1.00		
	bond d	0.52	0.51	0.51		
	bond e	0.11	0.25	0.26		
	bond f	0.11	0.25	0.26		
	bond g	0.52	0.51	0.51		
S_{conf}, cal K^{-1} mol^{-1}		8.08	9.01	9.05	7.12	7.51
U_{conf}, kcal mol^{-1}		−0.31	−0.16	−0.14	−0.76	−0.43
ΔS_u,[d] cal K^{-1} mol^{-1}			14.1	13.1		11.6
ΔH_u,[d] kcal mol^{-1}			7.2 ± 0.5	6.88		6.41
bond length, Å	$l_{O-C(=O)}$	1.354				
	$l_{C(=O)-C(=O)}$[e]	5.779				
	l_{O-CH_2}	1.445				
	$l_{CH_2-CH_2}$	1.525				
bond angle, deg	∠OC(=O)C(=O)	114.1				
	∠C(=O)OCH_2	116.2				
	∠OCH_2CH_2	110.0				
	∠$CH_2CH_2CH_2$	115.0				
dihedral angle, deg	ϕ_{cis}(C(=O)−C(=O))	180.0				
	$\phi_{g\pm}$ (O−CH_2)	±89.6				
	$\phi_{g\pm}$ (CH_2−CH_2)	±115.7				

[a] Using the conformational energies (Table 4) at the MP2/6-311+G(2d, p) level for benzene environments at 25 °C (for data at 25 °C) and 510 K (for data at 510 and 525 K) and the geometrical parameters (Table S3, Supporting Information) of trimethyleneglycol bis(dimethyl terephthalate). [b] Reference 2. [c] Equilibrium melting points. [d] Experimental values of entropy (ΔS_u) and enthalpy (ΔH_u) of fusion (refs 29 and 30). [e] The virtual bond for the terephthaloyl ring (see Figure 1).

dimer, an excimer, or an exciplex has been a subject of controversy.[19−22] This paper avoids discussing what the fluorescent species is and refers to it as 'dimer', in which photoinduced energy transfer occurs as a result of a close contact between two neighboring phenyl (terephthaloyl) groups. Our discussion is based on a simple principle that the I_D/I_M ratio would increase with existing probabilities of conformers satisfying geometrical conditions for the dimer formation.

Figure 6 expresses conformer probabilities of (a) TMGDB and (b) EGDB as a function of the $\overline{P_1P_2}$ distance and $\angle \mathbf{v}_1 \wedge \mathbf{v}_2$ angle. The distance distributions of TMGDB and EGDB are divided into two groups: TMGDB, 5.4−6.2 Å and 9.2−11.6 Å; EGDB, 7.5−8.4 Å and ∼11 Å. The 5.4−6.2 Å group of TMGDB is composed of the above-mentioned folding conformers: tg^+g^-t (existing probability = 0.03),[23] $tg^+g^-g^+$ (0.22), $tg^+g^-g^-$ (0.39), and $g^+g^+g^-g^-$ (0.02). Of these four, $tg^+g^-g^+$ and $tg^+g^-g^-$ have particularly high existing probabilities. The dimer formation can be initiated at not only the stationary points but also intermediate states between RISs; therefore, the RIS approximation is rather coarse for this problem. Accordingly, variations in geometrical parameters were introduced as follows. First, the maximum width ($\Delta\phi$) in a geometrical parameter (ϕ) was set. Second, random numbers were generated uniformly between [0, 1] and converted to values between $[\phi - \Delta\phi, \phi + \Delta\phi]$ of the geometrical parameter. Third, the $\overline{P_1P_2}$ distance and $\angle \mathbf{v}_1 \wedge \mathbf{v}_2$ angle were calculated with the geometrical parameters thus derived. As the standard geometrical parameters (ϕ's), those of PTT (Table 5) were used. The variations $\Delta\phi$'s in dihedral angles of bonds 5, 6, 7, and 8 were set at 10 or 20°, and all skeletal bond lengths and bond angles were, respectively, varied similarly within narrow ranges of ± 0.004 Å and ± 3.2°, which were estimated from Table S3 (Supporting Information). For each conformer, the samplings were repeated 10 000 times, and deviations from the equilibrium $\overline{P_1P_2}$ distance were individually calculated. The results are displayed as a histogram in Figure 7. The $\angle \mathbf{v}_1 \wedge \mathbf{v}_2$ angles of the four conformers with $\Delta\phi = 20°$ are widely distributed from 0 to 90° (when the $\angle \mathbf{v}_1 \wedge \mathbf{v}_2$ angle was larger than 90°, the supplement was taken); therefore, the angle distributions are not displayed here.

Here, the results will be examined against, for example, geometrical criteria for excimer formation. It has been suggested that the $\overline{P_1P_2}$ distance required for aromatic excimers ranges from 3 to 4 Å.[24,25] According to time-dependent density functional calculations for benzene dimers,[26] the excimer formation occurs only when $\overline{P_1P_2}$ is shorter than 5.5 Å. The excimer energy is minimized at 3.15 Å for the parallel arrangement ($\mathbf{v}_1 \| \mathbf{v}_2$) of benzene rings. Our histograms suggest possibilities that the four conformers may become intramolecular excimers even at $\Delta\phi = 10°$. Because the $tg^+g^-g^+$ and $tg^+g^-g^-$ conformers have the high existing probabilities, both TMGDB and PTT are expected to yield large I_D/I_M ratios. The 7.5−8.4 Å group of EGDB comprises tg^+t, tg^+g^+, tg^+g^-, $g^+g^+g^+$, and $g^+g^+g^-$ conformers. Similar simulations were carried out for these conformers but yielded no $\overline{P_1P_2}$ distances shorter than 4.9 Å even at $\Delta\phi = 20°$.[27] Probably, the I_D/I_M ratio closely correlates with the frequency and strength of close contacts between the phenyl (terephthaloyl) rings.

The experimental I_D/I_M ratios of PTT in dilute solutions show distinct solvent dependence: $I_D/I_M = 3.0$ in ethyl acetate, 1.2 in *p*-dioxane, 1.0 in dichloroethane, and 0.3 in trifluoroacetic acid (TFA).[17] Luo et al.[22] have also measured fluorescence spectra of PTT in a dilute solution of chloroform/TFA (4:1 v/v) mixed solvent, observed only the monomer emission, and concluded that neither interchain nor intrachain interactions are formed. We have suggested that acidic good solvents for PET, such as TFA, phenol, and trichlorophenol, strongly disturb its intramolecular attractions and, consequently, enlarge the chain dimension.[2] In fact,

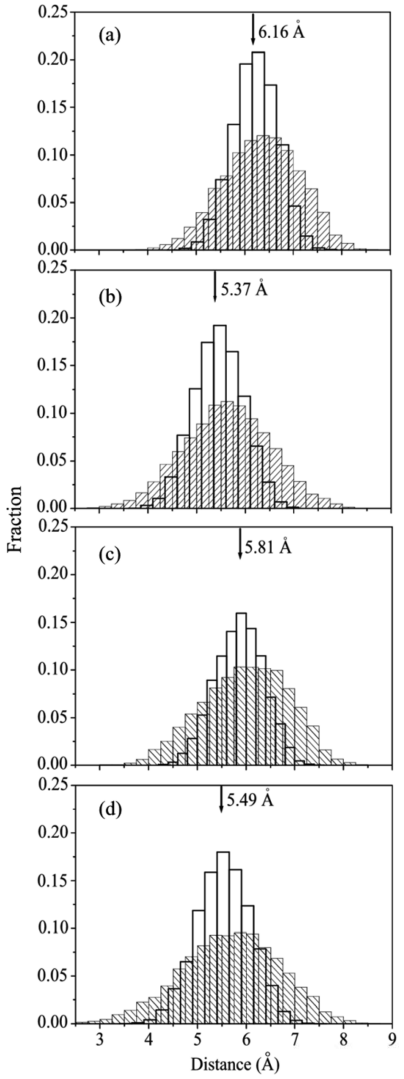

Figure 7. $\overline{P_1P_2}$ distance distributions of four folding conformers, (a) tg^+g^-t, (b) $tg^+g^-g^+$, (c) $tg^+g^-g^-$, and (d) $g^+g^+g^-g^-$, of TMGDB as a result of uniform variations of $[\phi - \Delta\phi, \phi + \Delta\phi]$ in dihedral angles of the skeleton: $\Delta\phi = 10°$ (open bars) and 20° (shaded bars). The vertical arrow indicates the equilibrium distance optimized at the B3LYP/6-311+G(2d, p) level.

characteristic ratios of unperturbed PET chains, estimated indirectly from extrapolation methods for viscometric measurements using the good solvents, are larger than those calculated from our refined RIS scheme and those determined from small-angle neutron scattering experiments for the melts. If the acid solvents affect the PTT chain similarly (for example, selective absorption to its ester group) and the above-mentioned intramolecular attractions are virtually ineffective, then the folding conformers would be exceedingly rare and the dimer emission would disappear. These inferences are entirely consistent with the experimental observations.

Configurational Properties and Thermodynamic Quantities of PTT. When all the higher-order intramolecular interactions, α_k's, of PTT are included in the refined RIS calculation,[28] the statistical weight matrices, U_j's, must be formulated in the form of 27 × 27. Accordingly, the original formulas developed for 9 × 9 U_j matrices have been partly revised: In eqs 1 and 2 of ref 28, the t_n value is set equal to 27. For bonds 8, a−g, and n, the M_γ (eq 8 of ref 28) and $\|T\|_\gamma$ (eq 13) matrices are extended by $I_3 \otimes M_\gamma$ and $I_3 \otimes \|T\|_\gamma$, respectively.

A virtual bond has been defined for the terephthaloyl ring of PTT; the line segment connecting two carbonyl carbons attached to the same terephthaloyl ring is treated as if to be a long C−C bond (bonds 3 and b in Figure 1). Statistical weight matrices of bonds 2−8 and a−g, formulated in the 27 × 27 form, are given in eqs 7−11 and the Appendix. Configuration-dependent parameters of PTT at 25 °C, 510 K, and 525 K were calculated from conformational energies for benzene environments at 25 °C, 510 K, and 510 K, respectively; two equilibrium melting points (T_m) of PTT, 510 and 525 K, have been reported.[29,30] The cis−trans energy difference (E_γ) of the terephthaloyl group was taken from that of dimethyl terephthalate.[2] The geometrical parameters used are shown in Table S3. The calculated results are listed in Table 5.

The characteristic ratios ($\langle r^2\rangle_0/nl^2$'s) of infinite unperturbed PTT chains (degree of polymerization, $x \rightarrow \infty$) at 25 °C, 510 K, and 525 K, determined from extrapolations to $x^{-1} \rightarrow 0$ of $\langle r^2\rangle_0/nl^2$ vs x^{-1} plots, are 1.37, 2.43, and 2.47, respectively.[31] For comparison, the corresponding data on PET[2] are partly shown in Table 5. The temperature coefficients ($10^3 d(\ln\langle r^2\rangle_0)/dT$) of PTT are much larger than those of PET; the overall temperature coefficients between 25 °C and T_m are 2.6−2.7 K^{-1} (PTT) and 0.34 K^{-1} (PET). To our knowledge, no experimental $\langle r^2\rangle_0/nl^2$ value of PTT has been reported up to the present. If the $\langle r^2\rangle_0/nl^2$ ratio were obtained from the Stockmayer−Fixman plot[32] for PTT dissolved in the acidic good solvent(s), the intramolecular attractions would be strongly disturbed. If we consider the MP2 energies (Table 3) to represent the PTT chain maintaining the intramolecular attractions as they are, we can calculate the characteristic ratio at 25 °C as 1.37; on the other hand, if we consider the HF energies to express PTT losing the attractions completely, we may estimate the $\langle r^2\rangle_0/nl^2$ value at 25 °C to be 6.54 (not given in Table 5). Therefore, the Stockmayer−Fixman extrapolation for viscometric measurements using the acidic solvents would yield an in-between $\langle r^2\rangle_0/nl^2$ value. This is a serious dilemma in polymer solution theory: the dissolution itself drastically alters the nature of the polymer.

The configurational entropy (S_{conf}) and intramolecular energy (U_{conf}) per monomer mole are given by[2,8]

$$S_{conf} = \frac{R}{x}\left[\ln Z + T\frac{d(\ln Z)}{dT}\right] \tag{17}$$

and

$$U_{conf} = \frac{RT^2}{x}\frac{d(\ln Z)}{dT} \tag{18}$$

The partition function of the whole chain, Z, is calculated from

$$Z = J^*\left(\prod_{j=2}^{n-1} U_j\right)J \tag{19}$$

where J^* is the row matrix of which first element is unity and the others are null, and J is the column matrix whose elements are unity. The S_{conf} and U_{conf} values, respectively, correspond to the configurational entropy and intramolecular energy of the Θ state relative to the crystalline state at a temperature T. The crystal is assumed to be defect-free; therefore, $S_{cryst} = 0$ and $U_{cryst} = 0$.

At the equilibrium melting point, T_m, the enthalpy ΔH_u and entropy ΔS_u of fusion are related by

$$\Delta H_u = T_m \Delta S_u \tag{20}$$

In Table 5, the S_{conf} and U_{conf} values of PTT, calculated from eqs 17 and 18, are given, together with experimental

ΔH_u and ΔS_u data.[29,30] The $S_{conf}/\Delta S_u$ ratio of PTT, a measure of intrachain effects on the overall structural change on melting, is 0.64 (510 K) or 0.69 (525 K), being comparable to that (0.65) of PET. The U_{conf} value of PTT is negative (−0.16 or −0.14 kcal mol^{-1}), but its magnitude is smaller than that (−0.43 kcal mol^{-1}) of PET. On the equilibrium crystallization of PTT at 510 (525) K, the configurational entropy decreases by 9.01 (9.05) cal K^{-1} mol^{-1}, and the internal energy increases by 0.16 (0.14) kcal mol^{-1}; the PTT chain itself acquires no thermodynamic advantage from the crystallization.[33] Therefore, some effective interchain stabilizations must compensate for the intrachain factors. In fact, PET (crystal conformation, ttt),[34] PTT (tggt),[35] and poly(butylene terephthalate) ($g^+g^+tg^-g^-$ for α form)[36] crystallize to form close contacts and parallel arrangements between the terephthaloyl rings, that is, intermolecular $\pi-\pi$ stackings. Note that the crystal conformationof PTT would be a stable state without the attractive interactions (ΔG_k(HF) = 0.38 kcal mol^{-1}, Table 3). This is in principle consistent with the RIS calculations (p_t = 0.52 for O−CH_2 and 0.11 for CH_2−CH_2 at 25 °C, Table 5) and expressed by the U_{conf} value smaller in magnitude than that of PET, whose p_t values are 0.49 for O−CH_2 and 0.05 for CH_2−CH_2 at 25 °C.[2] In crystallization of PTT, the intramolecular $\pi-\pi$ interactions formed densely in the molten (amorphous) state must be shifted by activated molecular motions to the intermolecular ones, and, simultaneously, the spacer is released from the folding conformations.

Conclusions

Conformational characteristics and configurational properties of PTT have been investigated by ab initio MO calculations and ^{1}H and ^{13}C NMR experiments for TMGDB and the refined RIS calculations for PTT. The MO calculations exactly reproduced experimental observations of NMR, dipole moment, and molar Kerr constant of TMGDB. Intramolecular interactions such as $\pi-\pi$ interactions, electrostatic attractions, and dipole−dipole interactions are formed in TMGDB (PTT) as a result of close contacts between the adjacent phenyl (terephthaloyl) groups and considerably stabilize their folding conformations with $g^{\pm}g^{\mp}$ sequences at the center of the spacer. Of the folding states, $tg^+g^-g^+$ and $tg^+g^-g^-$ conformations, existing at high probabilities, may be sources of dimer fluorescent emission characteristic of TMGDB and PTT. The chain configuration of PTT in solutions would be subject to solvent effects. On the other hand, the short spacer of PET does not allow the neighboring terephthaloyl groups to interact with each other, and hence the dimer fluorescence is scarcely observed from its dilute solutions. Because PTT as well as PET form a number of complicated intramolecular attractive interactions, their spacer conformations can not be simply interpreted on the analogy of those of the corresponding polyethers, poly(trimethylene oxide) and poly(ethylene oxide). The small difference between PET and PTT, that is, whether the number of methylene units is 2 or 3, is amplified by the weak attractive interactions to be observed as a variety of dissimilarities in structures and properties.

Appendix

Statistical Weight Matrices of TMGDB and PTT. For the bond numbers, see Figure 1. The U_5-U_8 matrices are given in eqs 7−11.

$$U_1 = \begin{bmatrix}1\\0\\0\end{bmatrix}\otimes[1 \quad 1 \quad 1] \tag{A1}$$

$$U_2 = \begin{bmatrix}1\\1\\1\end{bmatrix}\otimes[1 \quad 0 \quad 0] \tag{A2}$$

$$U_3 = \begin{bmatrix}1\\0\\0\end{bmatrix}\otimes[1 \quad \gamma \quad 0] \tag{A3}$$

$$U_4 = \begin{bmatrix}1\\1\\0\end{bmatrix}\otimes[1 \quad 0 \quad 0] \tag{A4}$$

$$U_a = \begin{bmatrix}1\\1\\1\end{bmatrix}\otimes I_3\otimes I_3\otimes[1 \quad 0 \quad 0] \tag{A5}$$

$$U_b = \begin{bmatrix}1\\1\\1\end{bmatrix}\otimes I_3\otimes \begin{bmatrix}1&0&0\\0&0&0\\0&0&0\end{bmatrix}\otimes[1 \quad \gamma \quad 0] \tag{A6}$$

$$U_c = \begin{bmatrix}1\\1\\1\end{bmatrix}\otimes \begin{bmatrix}1&0&0\\0&0&0\\0&0&0\end{bmatrix}\otimes \begin{bmatrix}1&0&0\\0&1&0\\0&0&0\end{bmatrix}\otimes[1 \quad 0 \quad 0] \tag{A7}$$

$$U_d = \begin{bmatrix}1\\0\\0\end{bmatrix}\otimes \begin{bmatrix}1&0&0\\0&1&0\\0&0&0\end{bmatrix}\otimes \begin{bmatrix}1&0&0\\0&0&0\\0&0&0\end{bmatrix}\otimes[1 \quad \rho \quad \rho] \tag{A8}$$

$$U_e = \begin{bmatrix}1\\1\\0\end{bmatrix}\otimes \begin{bmatrix}1&0&0\\0&0&0\\0&0&0\end{bmatrix}\otimes I_3\otimes[1 \quad \sigma \quad \sigma] \tag{A9}$$

$$U_f = \begin{bmatrix}1\\0\\0\end{bmatrix}\otimes I_3\otimes I_3\otimes[1 \quad \sigma \quad \sigma] \tag{A10}$$

$$U_g = U_8 \tag{A11}$$

$$U_n = \begin{bmatrix}1\\1\\1\end{bmatrix}\otimes I_3\otimes I_3\otimes[1 \quad 1 \quad 1] \tag{A12}$$

Supporting Information Available: Dipole moments and polarizabilities of conformers of TMGDB (Tables S1 and S2) and geometrical parameters used in the refined RIS calculations for PTT (Table S3). This material is available free of charge via the Internet at http://pubs.acs.org.

References and Notes

(1) For example : Chuah, H. H. *J. Polym. Sci., Part B: Polym. Phys.* **2002**, *40*, 1513 and references therein.
(2) Sasanuma, Y. *Macromolecules* **2009**, *42*, 2854.
(3) Frisch, M. J.; Trucks, G. W.; Schlegel, H. B.; Scuseria, G. E.; Robb, M. A.; Cheeseman, J. R.; Montgomery, J. A., Jr.; Vreven, T.; Kudin, K. N.; Burant, J. C.; Millam, J. M.; Iyengar, S. S.; Tomasi, J.; Barone, V.; Mennucci, B.; Cossi, M.; Scalmani, G.; Rega, N.; Petersson, G. A.; Nakatsuji, H.; Hada, M.; Ehara, M.; Toyota, K.; Fukuda, R.; Hasegawa, J.; Ishida, M.; Nakajima, T.; Honda, Y.; Kitao, O.; Nakai, H.; Klene, M.; Li, X.; Knox, J. E.; Hratchian, H. P.; Cross, J. B.; Bakken, V.; Adamo, C.; Jaramillo, J.; Gomperts, R.; Stratmann, R. E.; Yazyev, O.; Austin, A. J.; Cammi, R.; Pomelli, C.; Ochterski, J. W.; Ayala, P. Y.; Morokuma, K.; Voth, G. A.; Salvador, P.; Dannenberg, J. J.; Zakrzewski, V. G.; Dapprich, S.; Daniels, A. D.; Strain, M. C.; Farkas, O.; Malick, D. K.; Rabuck, A. D.; Raghavachari, K.; Foresman, J. B.; Ortiz, J. V.; Cui, Q.; Baboul, A. G.; Clifford, S.; Cioslowski, J.; Stefanov, B. B.; Liu, G.; Liashenko, A.; Piskorz, P.; Komaromi, I.; Martin, R. L.; Fox, D. J.; Keith, T.; Al-Laham, M. A.; Peng, C. Y.; Nanayakkara, A.; Challacombe, M.; Gill, P. M. W.; Johnson, B.; Chen, W.; Wong, M. W.; Gonzalez, C.; Pople, J. A *Gaussian03*, revision D.01. Gaussian, Inc.: Wallingford CT, 2004.
(4) Cances, E.; Mennucci, B.; Tomasi, J. *J. Chem. Phys.* **1997**, *107*, 3032.
(5) Mennucci, B.; Cances, E.; Tomasi, J. *J. Phys. Chem. B* **1997**, *101*, 10506.
(6) The National Institute for Materials Science, Japan. The PolyInfo Database Home Page. https://polymer.nims.go.jp (accessed May 27, 2009).
(7) Budzelaar, P. H. M. *gNMR*, version 5.0; IvorySoft & Adept Scientific plc: Letchworth, U.K., 2004.
(8) (a) Sasanuma, Y.; Watanabe, A. *Macromolecules* **2006**, *39*, 1646. (b) Sasanuma, Y.; Watanabe, A.; Tamura, K. *J. Phys. Chem. B* **2008**, *112*, 9613.
(9) Buys, H. R.; Eliel, E. L. *Tetrahedron Lett.* **1970**, 2779.
(10) Anteunis, M. J. O.; Tavernier, D.; Borremans, F. *Heterocycles* **1976**, *4*, 293.
(11) Tvaroska, I.; Hricovini, M.; Petrakova, E. *Carbohydr. Res.* **1989**, *189*, 359.
(12) Flory, P. J. *Statistical Mechanics of Chain Molecules*; Wiley & Sons: New York, 1969.
(13) Mattice, W. L.; Suter, U. W. *Conformational Theory of Large Molecules: The Rotational Isomeric State Model in Macromolecular Systems*; Wiley & Sons: New York, 1994.
(14) Mendicuti, F.; Rodrigo, M. M.; Tarazona, M. P.; Saiz, E. *Macromolecules* **1990**, *23*, 1139.
(15) Riande, E.; Saiz, E. *Dipole Moments and Birefringence of Polymers*; Prentice Hall: Englewood Cliffs, NJ, 1992 and references therein.
(16) Tsuzuki, S.; Honda, K.; Uchimaru, T.; Mikami, M.; Tanabe, K. *J. Am. Chem. Soc.* **2002**, *124*, 104 and references therein.
(17) Mendicuti, F.; Patel, B.; Viswanadhan, V. N.; Mattice, W. L. *Polymer* **1988**, *29*, 1669.
(18) Dodge, R. W.; Mattice, W. L. *J. Polym. Sci., Part B: Polym. Phys.* **1993**, *31*, 207.
(19) Allen, N. S.; McKellar, J. F. *Makromol. Chem.* **1978**, *179*, 523.
(20) Hemker, D. J.; Frank, C. W.; Thomas, J. W. *Polymer* **1988**, *29*, 437.
(21) Itagaki, H.; Inagaki, Y.; Kobayashi, N. *Polymer* **1996**, *37*, 3553.
(22) Luo, W.; Chen, Y.; Chen, X.; Liao, Z.; Mai, K.; Zhang, M. *Macromolecules* **2008**, *41*, 3912.
(23) The existing probability of conformer k was calculated as

$$M_k \exp(-\Delta G_k(\mathrm{MP2})/RT) / \sum_k M_k \exp(-\Delta G_k(\mathrm{MP2})/RT)$$

where ΔG_k(MP2) is the free energy at the MP2/6-311+G(2d, p) level of conformer k in benzene at 25 °C.
(24) Hirayama, F. *J. Chem. Phys.* **1965**, *42*, 3163.
(25) De Schryver, F. C.; Collart, P.; Vandendriessche, J.; Goedeweeck, R.; Swinnen, A.; Van der Auweraer, M. *Acc. Chem. Res.* **1987**, *20*, 159.
(26) Amicangelo, J. C. *J. Phys. Chem. A* **2005**, *109*, 9174.
(27) In our previous study,[2] no stationary points were found for folding conformers, $g^{\pm}g^{\mp}g^{\pm}$, of EGDB by geometrical optimization at the B3LYP/6-311+G(2d, p) level. However, this fact does not entirely deny the possibility that EGDB transiently approaches the folding states to be an intramolecular dimer.
(28) Sasanuma, Y.; Asai, S.; Kumagai, R. *Macromolecules* **2007**, *40*, 3488.
(29) (a) Pyda, M.; Boller, A.; Grebowicz, J.; Chuah, H.; Lebedev, B. V.; Wunderlich, B. *J. Polym. Sci., Part B: Polym. Phys.* **1998**, *36*, 2499. (b) Pyda, M.; Wunderlich, B. *J. Polym. Sci., Part B: Polym. Phys.* **2000**, *38*, 622.
(30) Chung, W.; Yeh, W.; Hong, P. *J. Appl. Polym. Sci.* **2002**, *83*, 2426.
(31) The characteristic ratio, calculated with bond lengths determined here (Table 5), should not be simply compared with those of other polymers, because the virtual-bond length is included in $\langle r^2\rangle_0/nl^2$ of PTT. The $\langle r^2\rangle_0/nl^2$ value, multiplied by nl^2/M (45.9/206 Å^2 g^{-1} mol) of the repeating unit, can be converted to $\langle r^2\rangle_0/M$.
(32) Stockmayer, W. H.; Fixman, M. *J. Polym. Sci., Part C* **1963**, *1*, 137.
(33) Of course, PTT is not expected to crystallize at T_m. The equilibrium crystallization is a gedanken experiment: PTT is melted at T_{up} ($> T_m$), cooled to T_m (state A, melt), cooled again to T_{down} ($< T_m$), completely crystallized there, and heated up to T_m (state B, crystal). Inasmuch as both intrachain entropy (S) and energy (U) are thermodynamic state functions that are dependent on temperature but independent of the process, their differences between states A and B, $S_B - S_A$ and $U_B - U_A$, correspond to $-S_{conf}$ (−9.01 or −9.05 cal K^{-1} mol^{-1}) and $-U_{conf}$ (+0.16 or +0.14 kcal mol^{-1}), respectively.
(34) Daubeny, R. de P.; Bunn, C. W.; Brown, C. J. *Proc. R. Soc. London, Ser. A* **1954**, *226*, 531.
(35) (a) Poulin-Dandurand, S.; Perez, S.; Revol, J. F.; Brisse, F. *Polymer* **1979**, *20*, 419. (b) Desborough, I. J.; Hall, I. H.; Neisser, J. Z. *Polymer* **1979**, *20*, 545.
(36) (a) Mencik, Z. *J. Polym. Sci., Polym. Phys. Ed.* **1975**, *13*, 2173. (b) Yokouchi, M.; Sakakibara, Y.; Chatani, Y.; Tadokoro, H.; Tanaka, T.; Yoda, K. *Macromolecules* **1976**, *9*, 266.